Acta Geotechnica (2011) 6:119–133
DOI 10.1007/s11440-011-0140-9

RESEARCH PAPER

DEM simulation of impact force exerted by granular flow on rigid structures

H. Teufelsbauer · Y. Wang · S. P. Pudasaini · R. I. Borja · W. Wu

Received: 25 January 2010 / Accepted: 19 May 2011 / Published online: 7 July 2011

Abstract The paper presents a DEM model for simulating dry granular avalanche down an incline. Flow pattern and impact forces on rigid obstacles are considered. Results of the simulations are compared with experimental data reported in the literature. The experiments include granular flow along an inclined channel and three-dimensional free surface flow on an inclined chute merging into a horizontal run-out region. The introduction of the rotation constraint allows realistic description of the flow behavior. Parametric studies are carried out to show the effect of model parameters on granular flow, including the run-out distance, deposition pattern, flow pattern, and impact forces against an obstacle.

Keywords Avalanche · DEM · Granular flow · Impact force

H. Teufelsbauer · Y. Wang · W. Wu (✉)
Institute of Geotechnical Engineering, University of Natural Resources and Life Sciences, Feistmantelstr. 4, 1180 Vienna, Austria
e-mail: wei.wu@boku.ac.at

Y. Wang
Department of Mechanical Engineering, Darmstadt University of Technology, Darmstadt, Germany

S. P. Pudasaini
School of Sciences, Katmandu University, Lalitpur, Nepal

R. I. Borja
Department of Civil and Environmental Engineering, Stanford University, Stanford, CA 94305-4020, USA

1 Introduction

Gravity-driven flows including snow avalanches and debris flows are dangerous natural hazards in alpine regions. Estimation of flow velocity, run-out distance, and impact force on protection structures of such flows is still a challenge. Practically proven and widely used snow avalanche and debris flow models are based on the principles of continuum mechanics for two-dimensional shallow flow down gently varying topographies in which the velocity distribution through the depth is assumed to be negligible [8, 19, 24, 34]. However, when there is a sudden change in field variables or topography, or when an obstacle is hit by the avalanche, these theories are too simplistic to accurately predict the flow dynamics in the vicinity of the obstacle. In practice, knowledge of avalanche velocities is usually sought around regions where intensive shear prevails, and where momentum transfer perpendicular to the sliding surface is significant. In these cases, three-dimensional extensions of the flow models are needed in order to accurately estimate the impact force on protection structures.

An alternative approach to continuum modeling is provided in this paper by a three-dimensional model based on discrete element method (DEM). DEM was introduced in geomechanics by Cundall and Strack [3] and was later adopted as a research tool by many other researchers [13, 17, 27, 30]. Since snow avalanche and debris flow can be regarded as granular flows [8, 18, 22, 34], DEM provides an ideal tool for modeling such phenomena. In comparison to continuum shallow flow models, the presented DEM model remains applicable to problems with complex topography and sudden change in field variables. Furthermore, the DEM approach allows accurate description of the flow dynamics with few material parameters.

There are only few publications in the literature on numerical simulation of the impact force exerted by granular flow against obstacles. Recently, the drag force of dilute granular flow was studied with the DEM by Bharadwaj et al. [1]. Well-documented laboratory experiments with dry sand were reported by Pudasaini et al. [20, 22, 23], Chiou [2], and Moriguchi et al. [16]. Teufelsbauer et al. [29] presented a DEM model for simulating dry granular avalanches. Impact force calculations of granular flows against structures are also presented by Montrasio and Valentino [15]. In this paper, the simulated impact forces on obstacles are calculated with the DEM, and the numerical results are compared with experimental data in the literature.

2 A DEM model for granular avalanche

The numerical calculations are carried out with the commercial software PFC3d (Particle Flow Code in three dimensions [9]). PFC3d is a simulation tool based on the DEM [2] and allows the computation of the dynamic motion and interaction of assemblies of arbitrarily sized spherical particles. The distinct elements, so-called balls, interact with each other based on a force–displacement law and Newton's second law of motion. Besides balls, PFC3d also provides wall elements, which allow the creation of static boundary elements. The displacements of colliding particles are represented by the overlap of the particles, and the interaction forces between the particles depend on the overlap. The forces between particles during contact are calculated according to some simple mechanical models such as springs and dashpots [4, 12, 14]. Usually, the contact force is decomposed into a normal component and a shear component. The material properties of the discrete elements (balls and walls) are characterized by the stiffness and friction. In addition, the balls are characterized by the ball radii and densities. The influence of various DEM parameters to the system behavior was investigated in former studies [2, 4, 25, 26, 28, 31, 32].

The normal and shear forces between particles and between particles and the wall are governed by the Kelvin–Voigt model. This model consists of an elastic spring and a viscous damper connected in parallel. The viscous damping controls the energy dissipation during particle collision and can be related to the restitution coefficient of granular materials. Both the normal and shear forces are subjected to some restrictions. For cohesionless granular materials, the normal force is restricted to be compressive only, i.e., tensile normal force is not allowed. The allowable tangential force is assumed to obey the Coulomb friction law, which can be expressed by a linear relationship between the normal force F^n and the allowable shear force $F^s_{\max}$ of the form

$$F^s_{\max} = \mu |F^n| \tag{1}$$

where μ is the friction coefficient. Slip between two adjacent particles occurs if the shear force is equal to the allowable shear force. In the presented granular flow model, internal and basal friction angles determined in the laboratory are assigned to the DEM parameters. In general, the DEM parameters differ from laboratory measurements [9]. However, in the case of rapid granular flows, Coulomb sliding friction is dominated by rotational friction, which allows a rough estimation of internal and basal friction.

The local damping, which defines a drag force to the particles, is set equal to zero in our numerical studies since the surrounding air has vanishingly small influence on the granular avalanche flow in laboratory scale.

An additional rotation control is added to the DEM model describing the rotation behavior of arbitrarily shaped granules with a rough surface by spherical DEM balls [11, 29, 33]. Without any rolling friction, the friction μ is not strong enough to prevent the particles from rolling down an incline. As a result, the model would strongly underestimate bed and internal friction angles measured in the laboratory. By means of the rotation model, it is possible to simulate gravity-driven flows of granular material realistically by DEM. The mechanism of rotation control used in this paper is described in detail by Teufelsbauer et al. [29]. Two parameters, the retarding time λ and the parameter χ, have to be identified to describe the rotational behavior of the particles. The retarding time λ defines the time span needed to reduce the angular velocity $\boldsymbol{\omega}$ about the retarding coefficient $k_\lambda = 1/(1 + c^\chi) \in [0, 1]$, where c is the number of contacts of a particle to its neighbor particles. If Δt is a discrete time step of the DEM calculation, the particle rotation ω_i^t in each direction $i = 1, 2, 3$ is reduced to give the new rotation ω_i^{t+1} for the following time step

$$\omega_i^{t+1} = k_\lambda^{\Delta t/\lambda} \omega_i^t \tag{2}$$

The retarding time is assumed to depend on the shear velocity v_s:

$$\lambda = k_v v_s + \lambda_c \tag{3}$$

The above expression for the retarding time λ is motivated by the observation that the influence of particle angularity decreases with increasing shear velocity. Hence, an additional shear-retarding coefficient k_v and a shear velocity-independent retarding time λ_c describe a linear relation between shear velocity and retarding time. If a particle is in contact with several particles, the mean of all shear velocities to the contacting particles is taken. This relation allows a more accurate description of the static deposition and dynamic flow of granular material with one mathematical model. The velocity-dependent retarding

time is especially important for three-dimensional free surface flows with unconfined run-out areas (see Fig. 1b).

Furthermore, the threshold velocity v_{sr} can be introduced when a particle passes from pure sliding to rolling. If the relative particle velocity is below the threshold velocity, the particle rotation is constrained to zero. This effect can often be observed in laboratory experiments when an angular particle slides along a smooth incline. When the particle begins to move, it is mostly sliding without rotation. If it has reached a certain (mostly stochastically varying) velocity, it begins to rotate. A similar effect can be observed in the deposition process. In general, the threshold velocity v_{rs} when an angular particle passes from rolling to pure sliding is much lower than the threshold v_{sr} caused by the kinetic energy of particle spin.

All presented material parameters are separately identified for internal and basal material behavior. If a differentiation is necessary, the superscript *bb* and *bw* is added to the parameters, denoting ball-ball and ball-wall contacts, respectively.

3 Evaluation of impact force against obstacles

The impact force of granular flow against obstacles has been the subject of some experimental investigations, which can be divided into two categories: quasi two-dimensional channel flow (Fig. 1a) and fully three-dimensional chute experiments flow (Fig. 1b). In channel experiments, the flow in lateral direction is confined by sidewalls with negligible small friction. Hence, the velocity gradients in lateral direction are marginal. Chute experiments allow the investigation of the influence of an obstacle to an unconfined free surface flow. When an avalanche hits a dam, it is deflected in lateral and basal surface normal direction.

The present DEM model allows the simulation of channel and chute flows and provides the possibility to evaluate normal and shear forces of the impact against a retaining wall. Therefore, the total force $F_b = \{F_i^b\}, \quad i = 1, 2, 3$ in each coordinate is evaluated by additional wall elements, which have the same location and dimension as the pressure plates in the real experiments. The total force is projected to normal forces F^n and shear forces F^s

$$\begin{aligned} F_i^n &= F_j^b n_j n_i, \quad \text{with } \|n\| = 1 \\ F_i^s &= F_i^b - F_i^n, \end{aligned} \tag{4}$$

where n is the normal vector of the pressure plate. The norm of the force vectors $\|F^s\|$ and $\|F^n\|$ gives the normal and shear force of the avalanche impact against the pressure plate, respectively.

3.1 Channel experiments

Moriguchi et al. [16] conducted a series of channel experiments with a length and width of 1.8 and 0.3 m for different inclination angles 45°, 50°, 55°, 60°, and 65°. The experiments were performed with 50 kg Toyoura sand with a bulk density of 1,379 kg/m^3 with minimum and maximum void

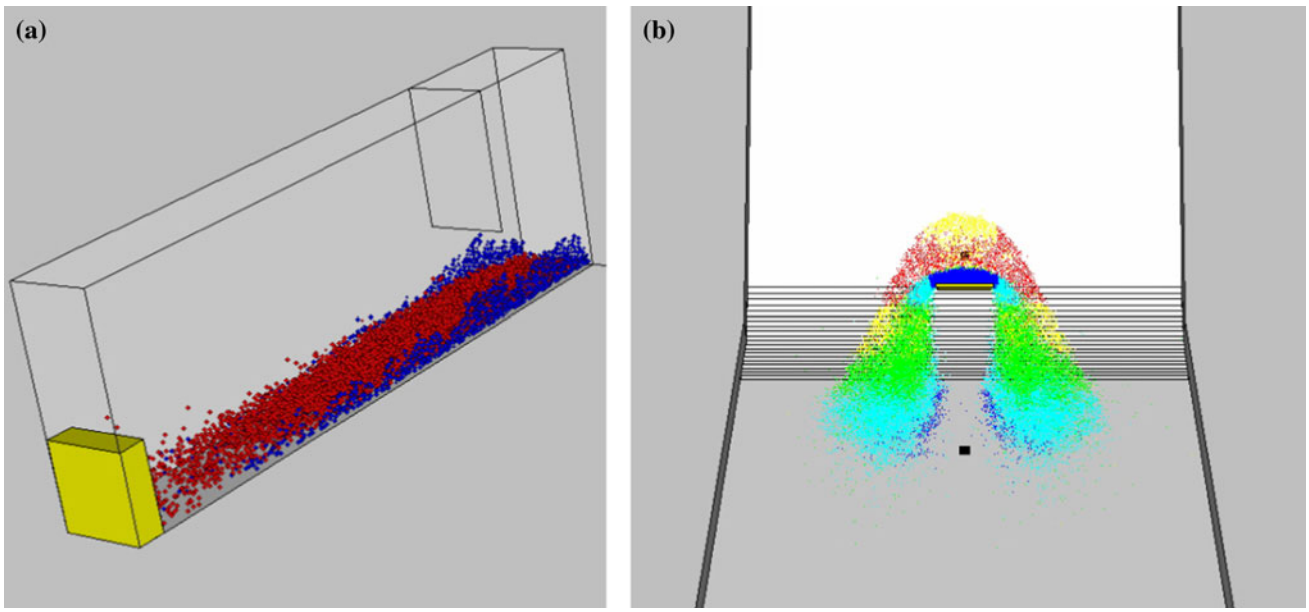

Fig. 1 Experimental setup: **a** channel flow experiment, **b** chute experiment

ratios of 0.61 and 0.97, respectively. The density of the solid phase is about 2,650 kg/m^3. The mean grain diameter is about 0.25 mm. The basal surface and the impact wall of the channel were coated with sand to provide higher surface friction. The side walls of the channel are made of Plexiglas with low friction. Basal and internal friction angles are not provided in [15]. However, for our simulations, a dynamic internal friction angle of 35° is assumed, which is usually measured for dry sand [2, 20–22].

One challenge in DEM modeling is the identification of model parameters. Particle properties like particle stiffness, damping coefficient, particle density, internal and basal friction angle, and rotation threshold velocities can be determined by laboratory experiments, whereas other parameters like contact influence and retarding times can not directly be obtained by laboratory experiments. A detailed description of parameter identification and their influence on the flow behavior of granular free surface flows is provided in our previous work [29].

In the laboratory experiment, the basal surface is coated with Toyoura sand to provide high surface friction. The side walls are smooth with very low friction in order to provide symmetry boundary conditions. Fifty kilograms of Toyoura sand is stored in a 30 × 30 × 50 cm box. When the front door of the box is suddenly opened, the sand flows down the channel and finally hits the pressure plate. The maximum impact force is strongly dependent on the inclination angle of the channel (see Fig. 4).

Our calculations show that basal surface condition (especially the threshold velocity v_{sr}^{bw}, the retarding time λ^{bw}, and the basal friction μ^{bw}) have strong influence on the impact behavior of the avalanche. The retarding time λ^{bw} describes a rotational friction. If the sliding surface has a very rough structure, retarding times should be assumed very small in comparison with a smooth sliding surface. In the experiments of Moriguchi et al. [16], the basal channel surface is very rough because it is coated with sand particles. Hence, the ball-wall retarding time is assumed to be zero.

Case studies CS1 and CS2 demonstrate the influence of rotation parameters ν^{bb}, λ^{bb}, and k^{bb} on the flow and impact behavior of granular material. These both cases are performed with free ball-wall rotation, whereas the ball-ball rotation is highly constrained in CS1 and free in CS2 (see Table 1, Fig. 2).

The colors of the PFC results shown in this paper are based on following color code. Dark blue indicates zero velocity, and velocities in the range (0, $0.25v_{\max}$), ($0.25v_{\max}$, $0.5v_{\max}$), ($0.5v_{\max}$, $0.75v_{\max}$), and ($0.75v_{\max}$, $1.0v_{\max}$) are colored in light blue, green, yellow, and

Table 1 Case study 1 to case study 3 present DEM parameter sets for sensitivity analysis of the rotation control model

Parameter	CS1	CS2	CS3	CS4
Contact stiffness (normal)	10^8 N/m	10^8 N/m	10^8 N/m	10^8 N/m
Contact stiffness (shear)	10^8 N/m	10^8 N/m	10^8 N/m	10^8 N/m
Particle density	2,650 kg/m^2	2,650 kg/m^2	2,650 kg/m^2	2,650 kg/m^2
Ball-ball friction μ^{bb}	0.7	0.7	0.7	0.7
Ball-wall friction μ^{bw}	∞	∞	∞	∞
Critical damping ratio (normal)	0.1	0.1	0.1	0.1
Critical damping ratio (shear)	0.0	0.0	0.0	0.0
Local damping	0.0	0.0	0.0	0.0
Start rotation threshold velocity (ball-wall) v_{sr}^{bw}	0.0 m/s	0.0 m/s	0.0 m/s	∞ m/s^2
Stop rotation threshold velocity (ball-wall) v_{rs}^{bw}	0.0 m/s	0.0 m/s	0.0 m/s	∞ m/s^2
Start rotation threshold velocity (ball-ball) v_{sr}^{bb}	∞ m/s	0.0 m/s	100 m/s	0 m/s^2
Stop rotation threshold velocity (ball-ball) v_{rs}^{bb}	∞ m/s	0.0 m/s	100 m/s	0 m/s^2
Shear retarding coefficient (ball-wall) k_v^{bw}	∞ s^2/m	∞ s^2/m	0.0 s^2/m	0.0 s^2/m
Velocity-independent retarding time (ball-wall) λ_s^{bw}	∞ s	∞ s	∞ s	5 10^{-3}s
Shear retarding coefficient (ball-ball) k_v^{bb}	0.0 s^2/m	∞ s^2/m	0.0 s^2/m	0.0 s^2/m
Velocity-independent retarding time (ball-ball) λ_s^{bb}	0.0 s	∞ s	0.0 s	8 10^{-2}s
Contact influence χ	0	0	0	0
Uniformly distributed ball diameter in mm [$r_{\min}$, $r_{\max}$]	[7, 9]	[7, 9]	[7, 9]	[7, 9]

Parameters in case study 4 present material properties according to the experiments of Moriguchi et al. [16]

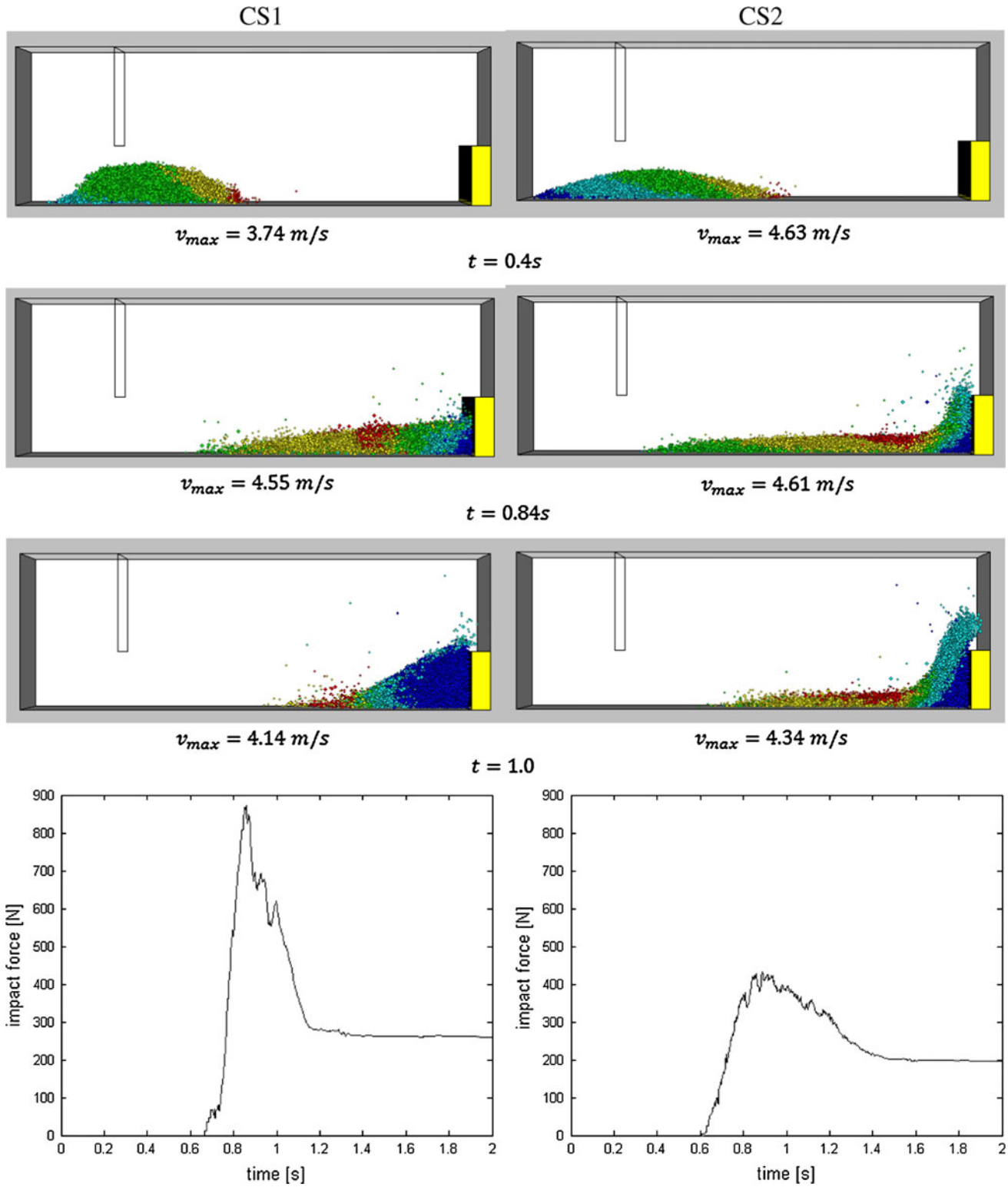

Fig. 2 Influence of particle rotation on the flow and impact behavior of granular flow. Both cases studies are performed with free ball-wall rotation, highly constrained ball-ball rotation in CS1, and free ball-ball rotation in CS2

red, respectively. The maximum velocity v_{max} is the maximum value of the magnitude of all the particle velocities evaluated in each time step. Time is given in seconds and velocities in m/s. About 9.000 particles are used in the PFC calculation for the shown channel experiments.

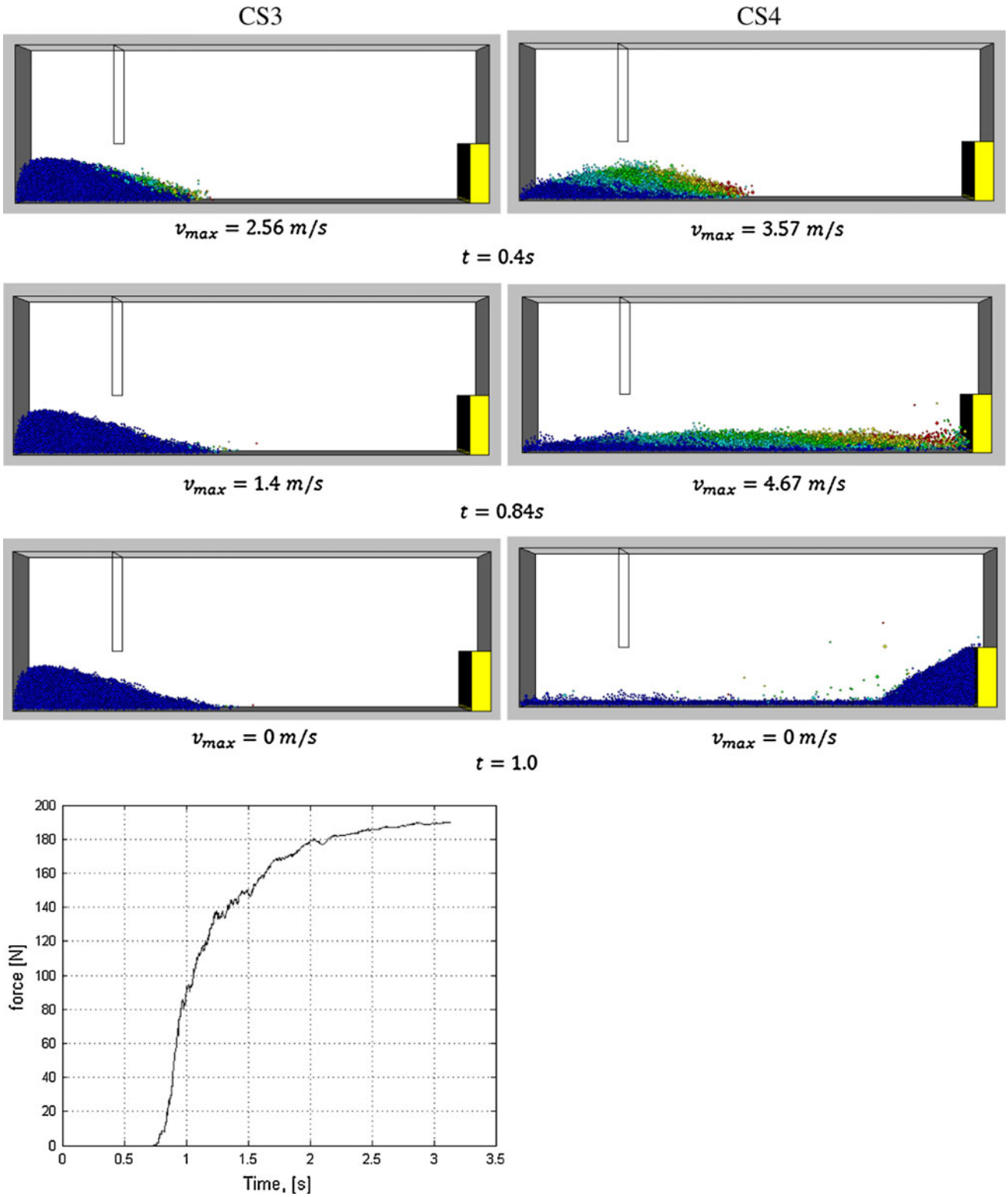

Fig. 3 Influence of particle rotation on the flow and impact behavior of granular flow. CS3 shows the case where particle rotation is completely constrained. CS4 shows the case where the particles are allowed to rotate

In CS3 and CS4, ball-ball rotation is investigated, while the particle rotation is constrained for ball-wall contacts. Therefore, one case study is performed with constrained ball-ball rotation and constrained ball-wall rotation (CS3), whereas in CS4 the ball-wall rotation is constrained and the ball-ball rotation is free (Fig. 3).

3.1.1 Conclusion of case studies 1–4

CS1 and CS2 clearly show that even for an extremely high Coulomb wall friction angle tan μ^{bw} much higher than the inclination of the channel, the granular flow along the inclined surface was accelerated very fast. Further numerical experiments show that for highly (CS4) or completely (CS3) constrained ball-wall particle rotation, the released granular material slides much slower or is even retained in the release area. However, CS1 and CS2 clearly show the influence of internal particle rotation. In both experiments, the Coulomb friction was assumed to be $\mu^{bb} = 0.7$. The simulation results show the different flow regimes and impact forces for constrained and free ball-ball rotation. If internal rotation is constrained (CS1), the released granular mass slides down the channel similarly to a rigid body. The avalanche body is relatively compacted from initiation till impact against the obstacle. If particle rotation is constrained, the internal friction is governed by the Coulomb sliding friction. Otherwise, if particles are free in rotation, Coulomb sliding friction is dominated by particle rotation, which drastically reduces shear resistance. As a consequence, in CS2, the granular flow can be redirected by the obstacles much easier than in CS1. In CS1, the whole kinetic energy is absorbed by the obstacle, whereas in CS2, a considerable portion of the avalanche flows over the dam. Hence, the maximal impact force in CS2 is much smaller than that in CS1, although travel and impact velocity of the granular flow are similar in both experiments. A comparison of the impact force computed in CS1 and CS2 with laboratory measurements Fig. 4 shows that in both case studies, the peak of the impact pressure is far too high. A reduction in the impact peak was reached by a reduction in ball-wall particle rotation as shown in CS4.

Figure 4 shows a comparison between laboratory experiments and simulated impact forces. It can be shown that the distinct element model is able to describe the flow and impact behavior of dry granular material reasonable well.

3.2 Chute experiments

In comparison to the channel experiments of Moriguchi et al. [16], the experiments of Chiou [2] and Pudasaini et al. [20] investigate three-dimensional free surface flows along an inclined chute merging into a horizontal run-out region. The impact forces against obstacles exerted by free surface flows were measured and described in detail by Chiou [2]. The chute with a width of 1.6 m has an inclined part with a length of 1.56 m, which merges into a horizontal part of 2.07 m. The transition between the inclined part and the horizontal run-out zone consists of a cylindrical transition zone with a length of 0.37 m. In the experiments, a dam with 20 cm width and 30 cm height was placed at the beginning of the transition zone (see Figs. 1b, 7). The challenge in modeling such three-dimensional free surface flow is to describe all the different flow regimes observed in experiments. The wall friction and particle rotation becomes very important in the DEM model [29] to describe the release behavior, the dense flow along the inclined chute, the impact with an obstacle, and finally, the deposition in the horizontal run-out zone. After the granular material is released from a hemispherical cap, the material starts to flow down the incline and spreads out in flow direction and lateral direction. The spreading of granulates depends strongly on the wall friction and on the constraint of ball-wall rotation. When the avalanche reaches the horizontal part of the chute, it is retarded by friction, and the mass is densely deposited over an elliptical area. The shape of the deposited material is mainly influenced by the ball-ball and ball-wall friction and rotation. If an obstacle is placed on the inclined chute, the flow is divided into two branches with some material retained in front of the obstacle. The granular mass is deposited in two long tails (see Fig. 7).

In laboratory experiments, a bi-directional stress gauge was placed at the front wall of the obstacle. The positions of the measurement and the chute geometry are presented in detail in [2]. The bi-directional pressure gauge is able to measure the normal stress N and shear stress S perpendicular and parallel to the wall, respectively. Two different test configurations are simulated in this paper. One experiment deals with granular flow without dam in order to evaluate the flow pattern and deposition area. Another experiment investigates the impact forces on the dam, which is placed at the beginning of the transition zone between the inclined plane and run-out zone.

Case studies 5 and 6 are performed for two different granular materials, quartz sand with a mean grain diameter of about 5 mm (CS5) and very fine yellow sand less than 1 mm diameter (CS6). Both materials have similar internal friction angles but different granular surface properties. The basal friction angle of quartz is lower than that of yellow sand. Further details about material properties are documented by Pudasaini et al. [20, 22, 23] and Chiou [2]. The particle diameter in the DEM model is uniformly distributed in the range of 4–6 mm for both materials in order to minimize the computation time. Consequently, a package of several 1,000 particles of yellow sand is represented by one DEM particle, whereas each quartz particle is modeled by one DEM particle. Further case studies investigate the influence of internal and basal particle rotation on the impact force. The DEM parameters for case studies 5–8 are given in Table 2. About 43,000 particles

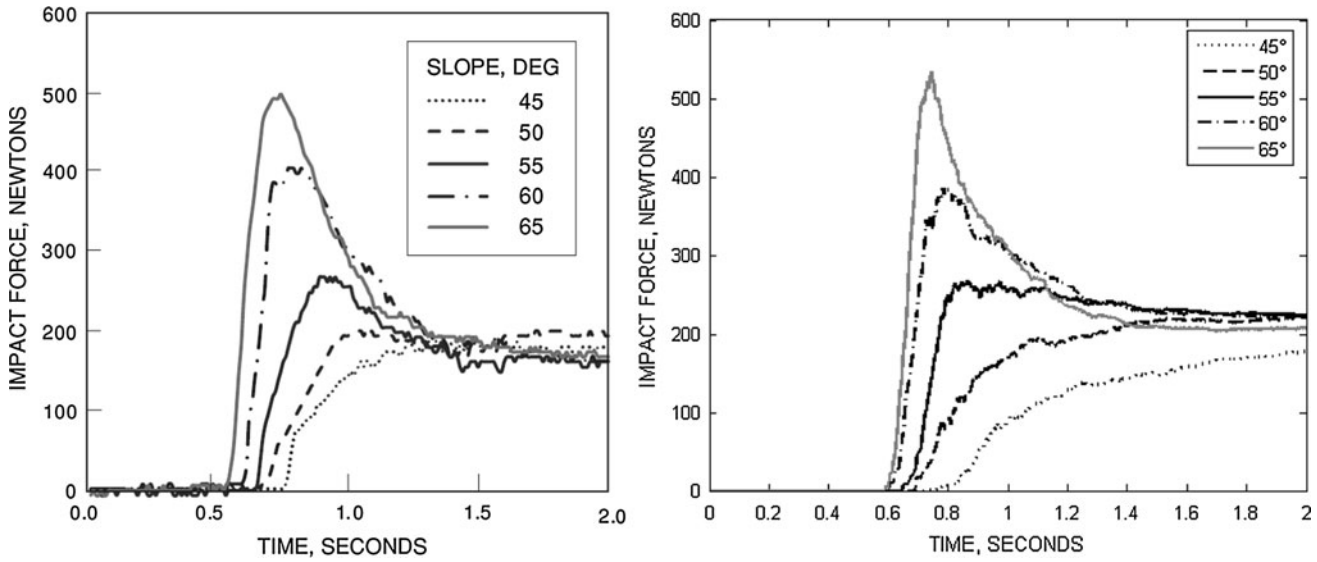

Fig. 4 *Left panel* time history of impact force for different channel inclinations measured in experiments by Moriguchi et al. [16], *right panel* simulated impact forces with parameter set CS4

Table 2 DEM parameter sets of chute experiments with quartz sand (case study 5) and yellow sand (case study 6)

Parameter	CS5	CS6	CS7	CS8
Contact stiffness (normal)	10^2 N/m	10^2 N/m	10^2 N/m	10^2 N/m
Contact stiffness (shear)	10^2 N/m	10^2 N/m	10^2 N/m	10^2 N/m
Particle density	2,970 kg/m^3	3,030 kg/m^2	3,030 kg/m^2	3,030 kg/m^2
Ball-ball friction μ^{bb}	0.84	0.84	0.84	0.84
Ball-wall friction μ^{bw}	0.47	0.53	0.53	0.53
Critical damping ratio (normal)	0.1	0.1	0.1	0.1
Critical damping ratio (shear)	0.0	0.0	0.0	0.0
Local damping	0.0	0.0	0.0	0.0
Start rotation threshold velocity (ball-wall) v_{sr}^{bw}	3.0 m/s	3.0 m/s	3.0 m/s	3.0 m/s
Stop rotation threshold velocity (ball-wall) v_{rs}^{bw}	0.1 m/s	0.1 m/s	0.1 m/s	0.1 m/s
Start rotation threshold velocity (ball-ball) v_{sr}^{bb}	0.0 m/s	0.0 m/s	0.0 m/s	0.0 m/s
Stop rotation threshold velocity (ball-ball) v_{rs}^{bb}	0.0 m/s	0.0 m/s	0.0 m/s	0.0 m/s
Shear retarding coefficient (ball-wall) k_v^{bw}	0.005 s^2/m	0.005 s^2/m	0.015 s^2/m	0.005 s^2/m
Velocity-independent retarding time (ball-wall) λ_s^{bw}	0.0 s	0.0 s	0.0 s	0.0 s
Shear retarding coefficient (ball-ball) k_v^{bb}	0.0 s^2/m	0 s^2/m	0 s^2/m	0 s^2/m
Velocity-independent retarding time (ball-ball) λ_s^{bb}	0.002 s	0.002 s	0.002 s	0.1 s
Contact influence χ	0	0	0	0
Uniformly distributed ball diameter in mm [$r_{\min}$, $r_{\max}$]	[2, 3]	[2, 3]	[2; 3]	[2; 3]

Case studies 7 and 8 show the influence of ball rotation in comparison to case study 6

are used in the PFC calculation for the shown chute experiments.

Before simulating the impact force on obstacle, the behavior of unimpeded granular flow will be investigated. The numerical simulation of unimpeded flow is compared with the experiments [20], where the flow was tracked by PIV (Particle Image Velocimetry). Figure 5 shows some snapshots of the flow pattern from PIV and DEM simulation.

A perusal of the experimental and numerical snapshots shows that the flow patterns from initiation till deposition are well reproduced by the numerical model.

Snapshots of PIV measurements in Fig. 6 and experimental results in Fig. 5 are not available for exactly the

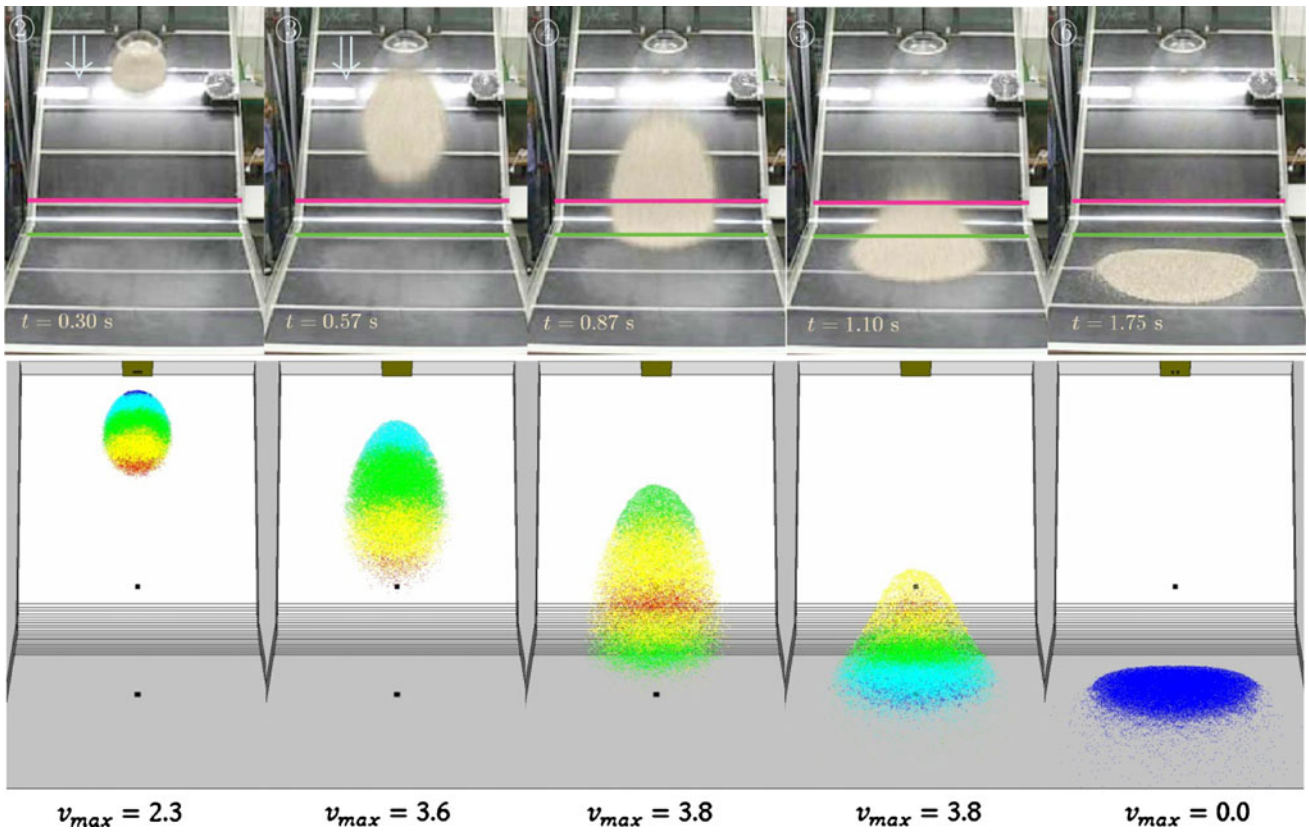

Fig. 5 Comparison of simulation results (CS5) and laboratory experiments [20]. Snapshots of the spreading of mass from initiation to final deposition is presented for $t = 0.3, 0.57, 0.87, 1.1, 1.75$. The colors in the simulation represent particle velocity with *dark blue* for null velocity, *light blue* for $(0, 0.25v_{max})$, *green* for $(0.25v_{max}, 0.5v_{max})$, *yellow* for $(0.5v_{max}, 0.75v_{max})$, *red* for $(0.75v_{max}, 1.0v_{max})$

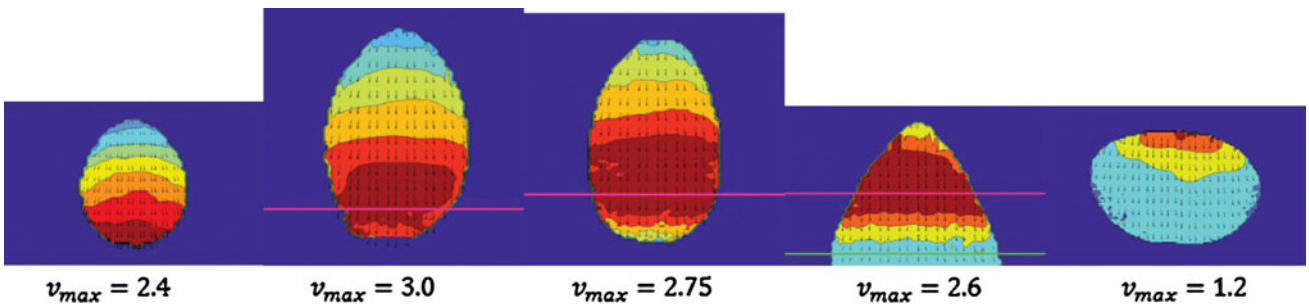

Fig. 6 PIV measurements [20] from laboratory experiments shown in the upper panel in Fig. 5 for $t = 0.38, 0.63, 0.69, 1.05, 1.25$. The colors in the simulation represent particle velocity with *dark blue* for null velocity, *light blue* for $(0, 0.25v_{max})$, *green* for $(0.25v_{max}, 0.5v_{max})$, *yellow* for $(0.5v_{max}, 0.75V)$, and *red* for $(0.75v_{max}, 1.0v_{max})$

same times. Hence, a direct comparison of Figs. 5 and 6 is not possible for all shown snapshots. Nevertheless, the comparison between PIV measurement and simulation result allows a rough evaluation of the surface velocities of the granular avalanche. The comparison shows that the simulated maximum velocities are up to 40% higher than the PIV measurement. This results from a different measurement method. The PIV measurement shows only the maximum flow velocity of the avalanche surface, whereas the DEM simulation evaluates the maximum flow velocity of all particles on the avalanche surface and within its body. If the color code is combined with the maximum velocities, PIV measurement and DEM simulations show similar characteristics.

The effect of particle rotation of the flow and deposition pattern of impeded flow is shown in Fig. 7. As might be

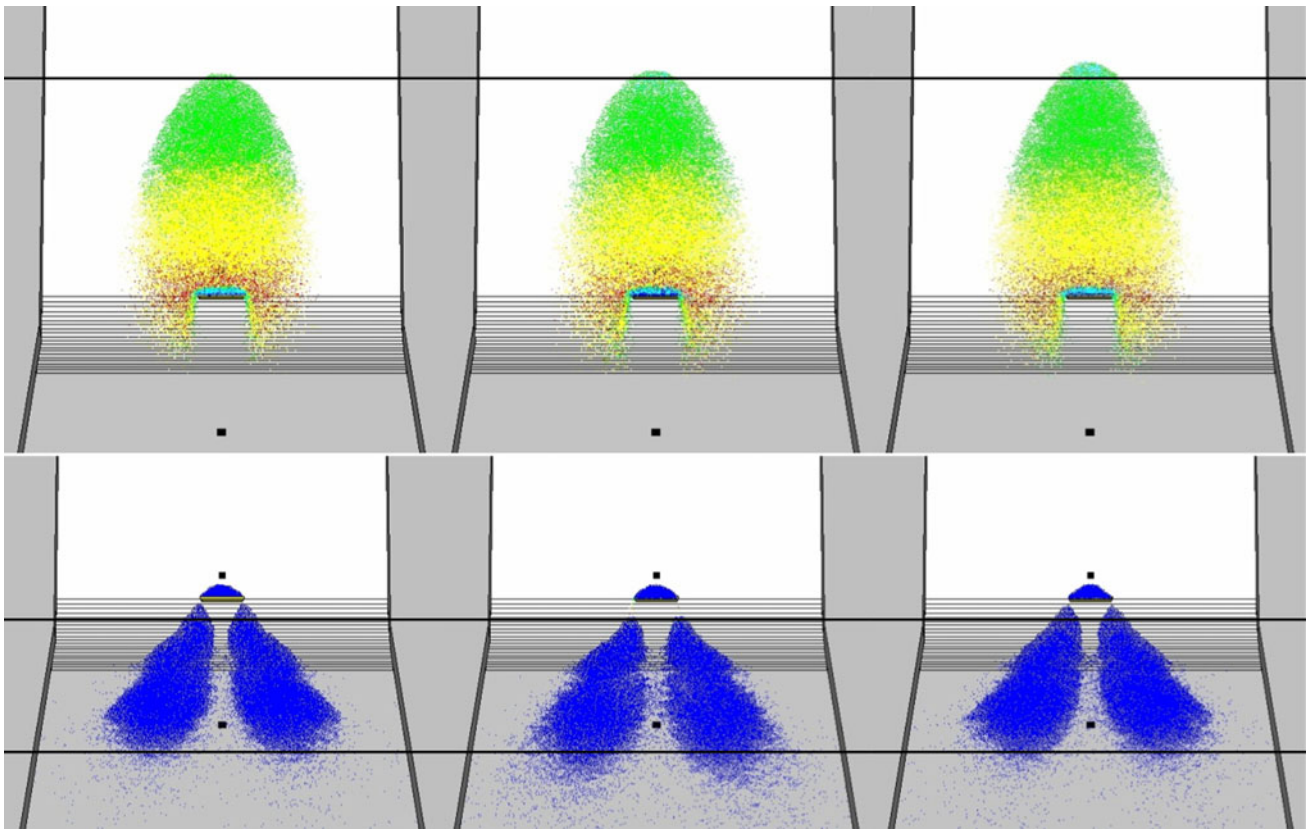

Fig. 7 The *left panel* shows the reference flow pattern for yellow sand (CS6), which was evaluated with laboratory experiments by Chiou [2]. The *middle* (CS7) and *right panels* (CS8) show the influence of variations in rotation parameters on the flow pattern and final deposition. The snapshots in the *upper row* are evaluated at $t = 0.74$ s and the lower row at $t = 5$ s

expected, the simulation with less rotation constraint gives rise to more scattered deposition. Figure 8 shows the influence of particle rotation and wall friction on the impact normal and shear force against obstacle. The maximum impact peak force depends mainly on the impact velocity and the mass of granular material that hits the obstacle. Moreover, the wall friction and ball-wall particle rotation have a significant influence on the flow behavior and the impact forces. From numerical experiments, it was found that a reduced constraint in particle rotation leads to a more scattered flow, especially in the run-out zone. An increase in wall friction stretches the avalanche in flow direction in the inclined part and leads to a shorter run-out distance in the horizontal part. The flow pattern and the final deposition in the run-out zone are strongly dependent on both parameters, the rotation constraint and the wall friction. If the released granular mass is widely stretched in flow direction, the mass is spatially dispersed, the impact duration becomes longer, and the peak impact force becomes smaller. Otherwise, if the released granular material flow is highly compacted, the whole released mass hits the obstacle within a short time and leads to a high impact peak force.

Our numerical simulations show that the flow pattern depends mainly on the basal friction and basal rotation properties. The effects of the variation of just one parameter on the impact force cannot be described in general. It depends strongly on whether basal friction is dominant or basal rotation is dominant in the current flow regime. However, in case study 5 and case study 6, it was shown that just the correlation of the basal friction parameter with laboratory measurements allows an accurate impact force simulation of quartz and yellow sand. A comparison of CS6 and CS7 in Fig. 8 shows that a small variation of basal ball rotation has only minor effects on the peak of the impact force but has noticeable effects on the scattering of the avalanche in the deposition zone (see Fig. 7). A further influence to the flow characteristics provides a variation of rotation constraint for ball-ball contacts (internal ball rotation). A particle is assigned to internal ball rotation if the particle has contacts to other particles but no contact to the wall. Otherwise, if a particle has wall contact, the constraint parameter of ball-wall rotation is assigned to the particle (basal ball rotation). An increase in internal ball rotation (compare CS 6 and CS 8) has only minor effects on the flow pattern and final deposition (Fig. 7) but leads to

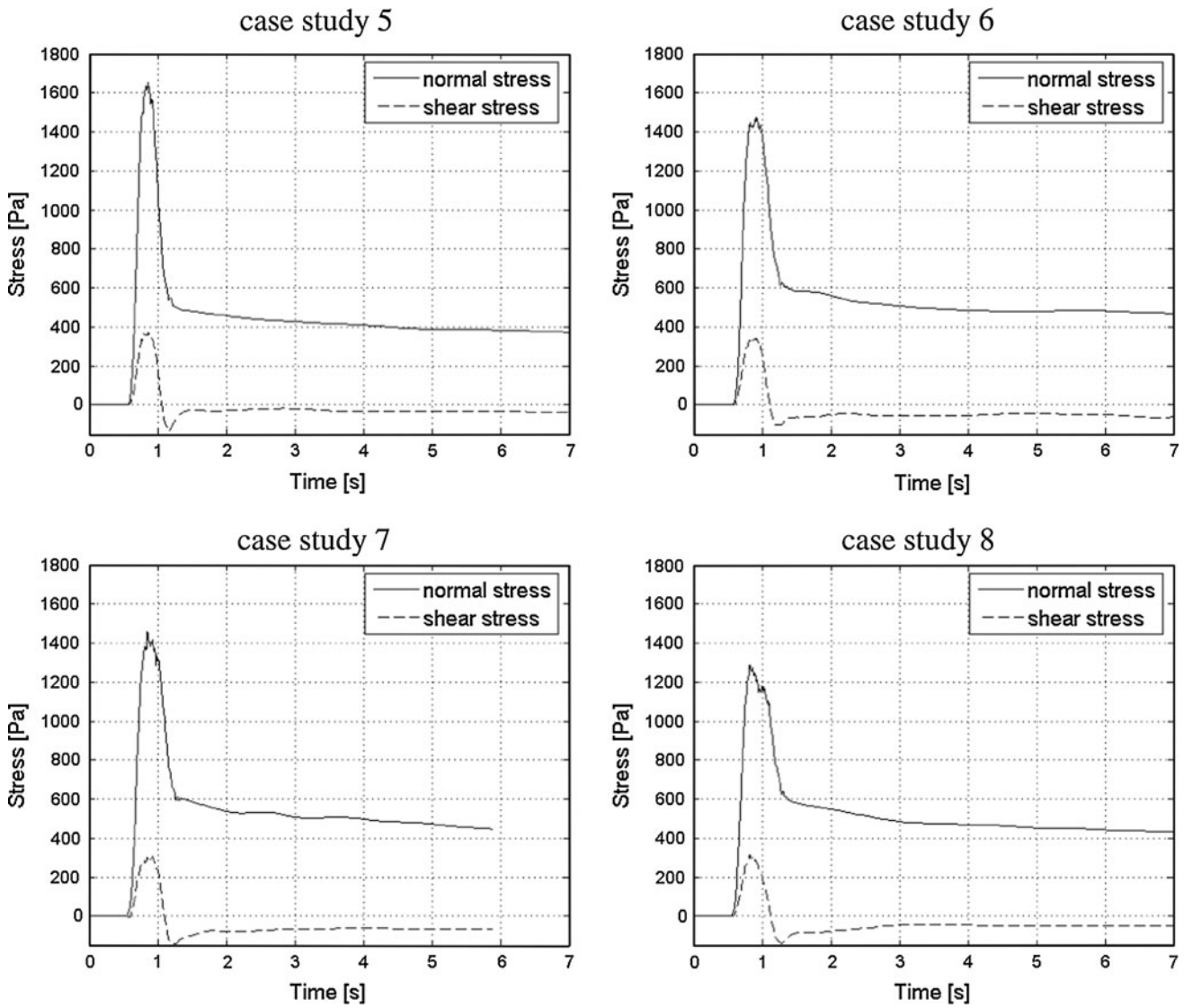

Fig. 8 Impact forces against obstacle for quartz (CS5) and yellow sand (CS6). CS7 and CS8 show the influence of basal (CS7) and internal (CS8) rotation parameters on the impact force

a decrease in impact force (Fig. 8). It is assumed that a higher internal particle rotation relieves the avalanche to be deflected in front of an obstacle. Hence, less kinetic energy has to be absorbed by the structure. Similar effects could be observed in Sect. 3.1 (CS1 and CS2). However, the right parameterization of material properties is very complex and was performed by a series of case studies for different chute types and obstacle positions.

3.3 Effect of multiple obstacles

Prevention structures constructed in the path of avalanches play an important role in the mitigation of avalanche hazards. The purpose of the prevention structures is to reduce or eliminate the hazard from potentially destructive avalanches. The present practice of snow prevention is largely based on the strategy of retention by massive defense structures such as snow bridges and embankments. While such defense structures have achieved certain success, their construction in Alpine terrains often requires the transportation by helicopter and is therefore rather cost-intensive. An alternative protection measure to the conventional large obstructions is expected by a large number of small obstacles, which are arranged in a matrix and tied down to the slope by ground anchors. While the massive retention structures attempt to hold up avalanches, a redistribution system aims at mixing and redistributing the snow layer in order to absorb the damaging energy and to reduce the hazard potential of avalanches. Despite the relatively small size of the

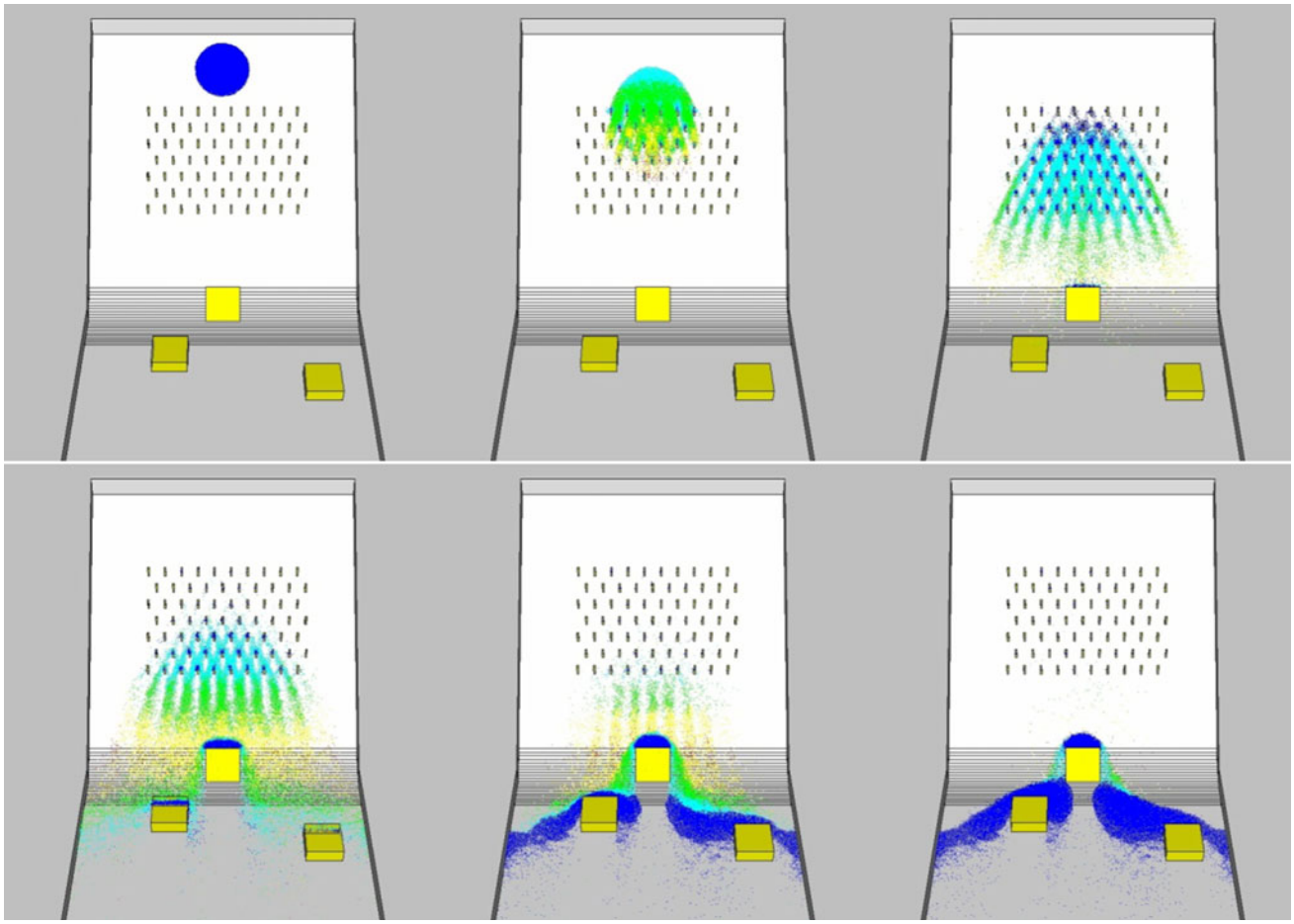

Fig. 9 Snapshot series ($\Delta t = 0.4$ s) of the interaction between protection structure matrix and avalanche

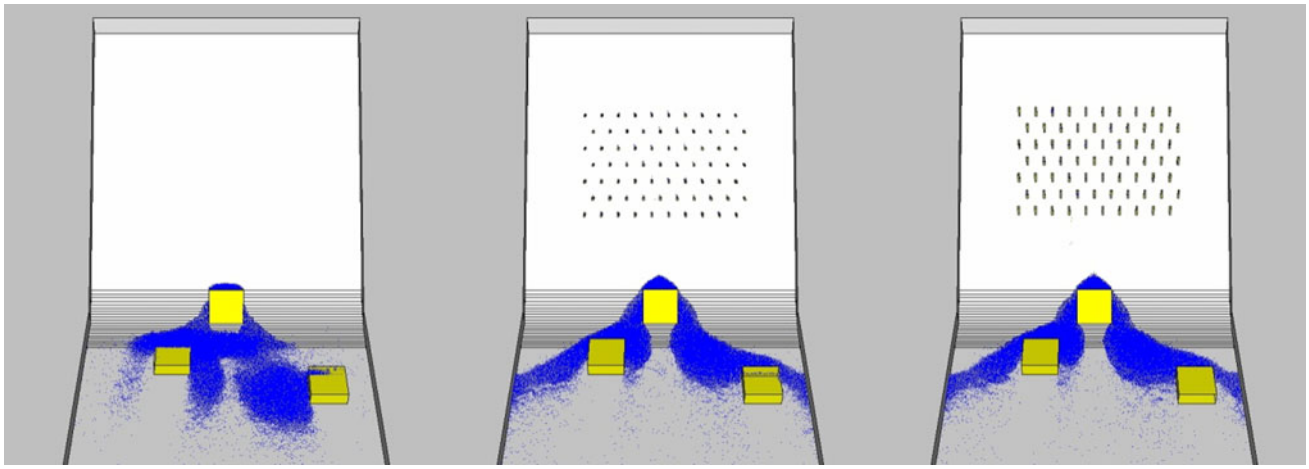

Fig. 10 Comparison of the final deposition for **a** unimpeded avalanche, **b** PSM with attack angle 110°, and **c** PSM with attack angle 45°

obstructions, a matrix of such obstructions shows additionally stabilizing effect of the snowpack and hence reduces the probability of avalanche ignitions. An advantage of such systems is the small size and light weight of the obstructions. The obstructions are prefabricated and can be transported and installed manually in most difficult terrains. Unlike the massive retention structures, the fall-out of an individual obstruction does

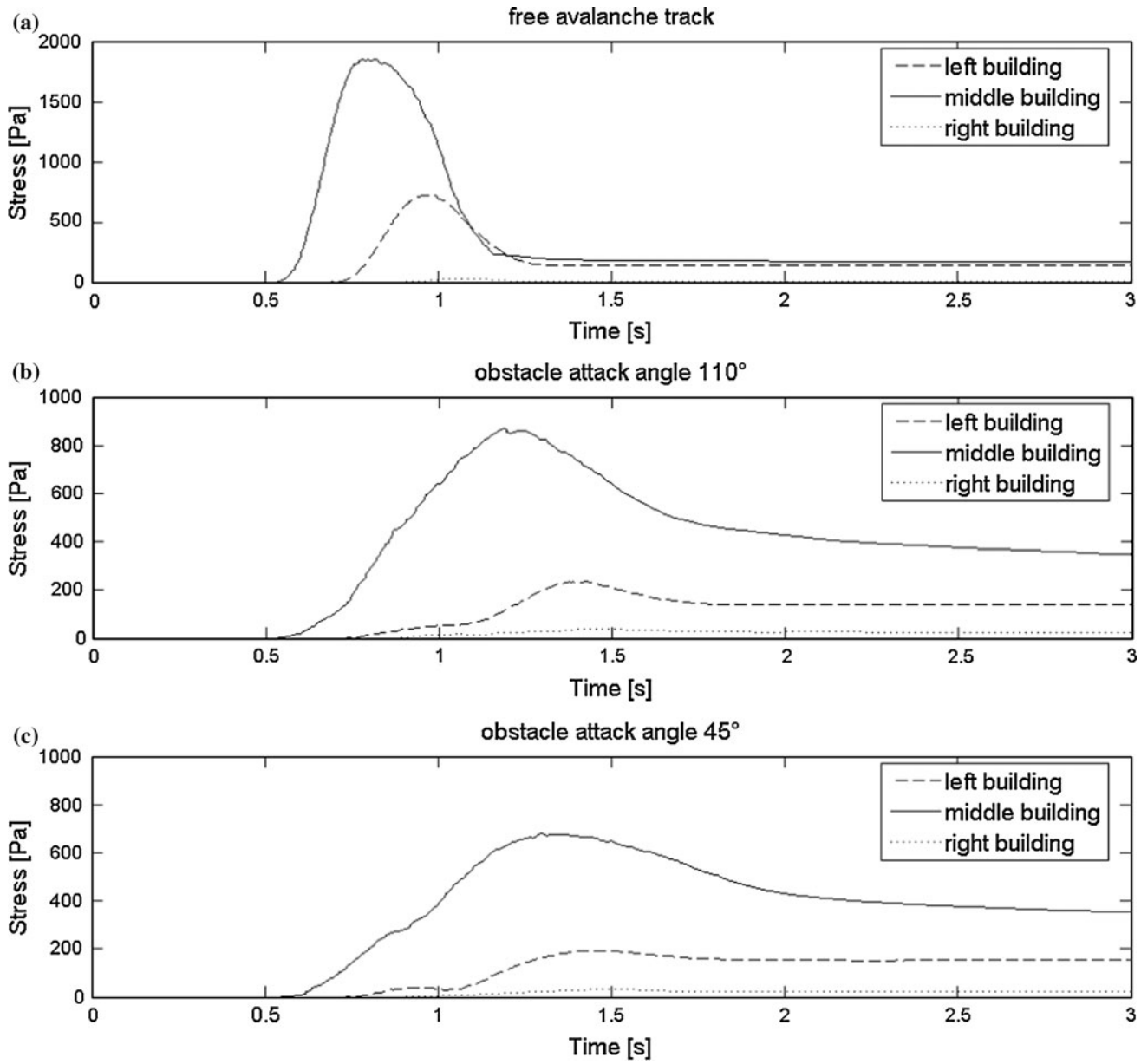

Fig. 11 Comparison of the impact force against the three buildings in normal direction for **a** unimpeded avalanche, **b** PSM with attack angle 110° and **c** PSM with attack angle 45°

not give rise to a system failure, which means higher reliability of the system.

In this section, some preliminary results of the interaction between granular and multiple obstacles are presented. In the numerical model, a matrix of obstacles (**P**rotection **S**tructure **M**atrix, PSM) is placed on a slope in front of three blocks, which simulate buildings. The simulation allows an evaluation of the forces acting on the obstacles of the PSM and the front walls of the buildings. Three case studies are presented. The first study presents the impact of the avalanche against the buildings without PSM. The other two studies investigate the protection of and the reduction in impact forces against the building by PSM. The influence of the attack angle of the obstacles on the protection effect of the PSM is compared in the last two experiments. The attack angle is defined as the angle between basal surface of the chute and the impact plane of the obstacle. The PSM used in the following case studies consists of 7 rows, each consisting of 10 obstacles with a cross section of 1 × 1 cm and a height of 5 cm. The distance between two obstacles in lateral direction is 9 cm, and the rows have a distance of 10 cm. The three buildings have a ground area of 20 × 20 cm and a height of 8 cm. The impact wall of the left house has a distance of 1.94 m from

the top corner of the chute, the middle house a distance of 1.56 m, and the right house a distance of 2.15 m. Measured from lateral symmetry axes of the chute, the left house is shifted 30 cm to the left, the right house 55 cm to the right, and the middle house is positioned in the symmetry axes.

Figure 9 shows some snapshots of the interaction between granular flow and PSM. The reduction in kinetic energy by the PSM is shown in Fig. 11 by the impact forces against obstacles. However, a negative effect of the PSM is the increased lateral scattering of the granular material (see Fig. 5). The comparison of the final deposition in Fig. 10 clearly points out that the attack angle of the obstacles has only minor effect on the lateral scattering of granular material. However, compared with the unimpeded avalanche track, the lateral scattering of the deposition is definitely higher if PSM is installed. However, the large reduction in kinetic energy by a PSM results in reduced impact forces in the boundary regions of the avalanche. The comparison of the impact forces in Fig. 11 clearly shows the influence of the attack angle of the obstacles on the performance of PSM. If the obstacles are placed vertically (Fig. 11c), the PSM shows better performance than obstacles with higher attack angle. The comparison of Fig. 11b and c shows that the influence of the attack angle on the impact peak force can reach about 20%. The simulations are based on parameter settings in CS5.

The comparison of the peak forces on the three buildings (Fig. 11) shows that the PSM has excellent protection capacity. The installation of PSM reduces the impact peak by a factor of about 2. If the obstacles are installed vertically (attack angle of 45°), the PSM shows better protection performance than the PSM with attack angle of 110°. The main reason for this effect is that the avalanche overflows the obstacles much easier for higher attack angle [5–7, 10]. Hence, less kinetic energy is absorbed by the obstacles, which results in higher impact forces against the buildings in the transition and the run-out zone.

4 Conclusion

In this paper, we have shown that the three-dimensional DEM is an appropriate tool for modeling granular flows and their interactions with obstacles. It is shown that the model performance is strongly dependent on the rotation control. Without any rotation constraint, the flow behavior of rough and angular granules cannot be described by DEM correctly. The comparison between numerical simulation and laboratory experiments for different channel inclinations and chute types shows good agreement. A comparison of impact forces and flow patterns with laboratory experiments indicates the potential applicability of the presented DEM avalanche model for a wide range of laboratory setups. Compared with depth averaged continuum approaches, the DEM is rather time consuming. However, DEM allows fully three-dimensional modeling of granular flows without geometrical restriction and averaging of field variables. This allows us to study the retention of protective structures, the impact forces on protective structures, and run-out and deposition behavior of granular flows.

Acknowledgment The authors are grateful to the Austrian Science Fund (FWF) for the grant L351: Numerical modelling of innovative protection against snow avalanches.

References

1. Bharadwaj R, Wassgren C, Zenit R (2006) The unsteady drag force on a cylinder immersed in a dilute granular flow. Phys Fluids 16:1511–1517
2. Chiou MC (2005) Modelling dry granular avalanches past different obstructs: numerical simulations and laboratory analyses. Dissertation, Technical University Darmstadt, Germany
3. Cundall PA, Strack ODL (1979) A distinct element model for granular assemblies. Geotechnique 29:47–65
4. Cundall PA (1988) Formulation of a three-dimensional distinct element model—Part I. A scheme to detect and represent contacts in a system composed of many polyhedral blocks. Int J Rock Mech Min Sci Geomech Abstr 25(3):107–116
5. Hákonardóttir KM, Hogg AJ, Jóhannesson T, Tómasson GG (2003) A laboratory study of the retarding effects of braking mounds on snow avalanches. J Glaciol 49(165):191–200
6. Hákonardóttir KM (2004) The interaction between snow avalanches and dams. PhD thesis, University of Bristol, School of Mathematics
7. Hákonardóttir KM, Hogg AJ (2005) Oblique shocks in rapid granular flows. Phys Fluids 17:077101. doi:10.1063/1.1950688
8. Hutter K, Wang Y, Pudasaini SP (2005) The Savage-Hutter avalanche model: how far can it be pushed? Philos Transact A Math Phys Eng Sci 363:1507–1528
9. Itasca Consulting Group, Inc. (2003) "PFC3D (Particle flow code in 3D) theory and background manual", Version 3.0, ICG, Minneapolis
10. Jóhannesson T (2001) Run-up of two avalanches on the deflecting dams at Flateyri, northwestern Iceland. Ann Glaciol 32:350–354
11. Khan KM, Bushell G (2005) Comment on ''Rolling friction in the dynamic simulation of sandpile formation''. Physica A 352:522–524
12. Kruggel-Emden H, Simsek E, Rickelt S, Wirtz S, Scherer V (2007) Review and extension of normal force models for the discrete element method. Powder Technol 171:157–173
13. Labra C, Rojek J, Oñate E, Zarate F (2008) Advances in discrete element modelling of underground excavations. Acta Geotech 3:317–322
14. Mindlin RD, Deresiewicz H (1953) Elastic spheres in contact under varying oblique forces. J. Appl. Mech. 20:327–344
15. Montrasio L, Valentino R (2004) Experimental and numerical analysis of impact forces on structures due to a granular flow. Manag Inf Syst 9:267–276
16. Moriguchi S, Borja RI, Yashima A, Sawada K (2009) Estimating the impact force generated by granular flow on a rigid obstruction. Acta Geotech 4(1):57–71
17. Muir Wood D, Maeda K (2008) Changing grading of soil: effect on critical states. Acta Geotech 3:3–14

18. Nicot F (2004) Constitutive modelling of snow as a cohesive-granular material. Granular Matter 6:47–60
19. Pitman EB, de Long LE (2005) A two-fluid model for avalanche and debris flows. Philos Transact A Math Phys Eng Sci 363:1573–1601
20. Pudasaini SP, Hsiau S, Wang Y, Hutter K (2005) Velocity measurements in dry granular avalanches using particle image velocimetry-technique and comparison with theoretical predictions. Phys Fluids 17(9)
21. Pudasaini SP, Hutter K, Hsiau S, Tai S, Wang Y, Katzenbach R (2007) Rapid flow of dry granular materials down inclined Chutes impinging on rigid walls. Phys Fluids 19(5)
22. Pudasaini SP, Hutter K (2007) Avalanche dynamics: dynamics of rapid flows of dense granular avalanches. Springer, Berlin
23. Pudasaini SP, Kroener C (2008) Shock waves in rapid flows of dense granular materials: theoretical predictions and experimental results. Phys Rev E 78(4)
24. Sampl P, Zwinger T (2004) Avalanche simulation with Samos. Ann Glaciol 38:393–398
25. Schwager T, Pöschel T (2007) Coefficient of restitution and linear–dashpot model revisited. Granular Matter 9:465–469
26. Schwager T, Pöschel T (2007) Coefficient of restitution for viscoelastic spheres: the effect of delayed recovery. arXiv:07081434
27. Sibille L, Donzé F-V, Nicot F, Chareyre B, Darve F (2008) From bifurcation to failure in a granular material: a DEM analysis. Acta Geotech 3:15–24
28. Stevens AB, Hrenya CM (2005) Comparison of soft-sphere models to measurements of collision properties during normal impacts. Powder Techn 154:99–109
29. Teufelsbauer H, Wang Y, Chiou M-C, Wu W (2009) Flow-obstacle-interaction in rapid granular avalanches: DEM simulation and comparison with experiment. Granular Matter 11(4), 209–220. doi:10.1007/s10035-009-0142-6
30. Thompson N, Bennett MR, Petford N (2009) Analyses on granular mass movement mechanics and deformation with distinct element numerical modeling: implications for large-scale rock and debris avalanches. Acta Geotech 4:233–247
31. Wu C, Li L, Thornton C (2003) Rebound behaviour of spheres for plastic impacts. Int J Impact Eng 28:929–946
32. Zhang J, Hu Z, Ge W, Zhang Y, Li T, Li J (2004) Application of the discrete approach to the simulation of size segregation in granular chute flow. Ind Eng Chem Res 43:5521–5528
33. Zhou YC, Wright BD, Yang RY, Xu BH, Yu AB (1999) Rolling friction in the dynamic simulation of sandpile formation. Physica A 269:536–553
34. Zwinger T (2000) Dynamik einer Trockenschneelawine auf beliebig geformten Berghängen. PhD Thesis, Vienna University of Technology